Tagging photon interactions at the LHC

X. Rouby[a*]

[a]Université catholique de Louvain, Center for Particle Physics and Phenomenology (CP3), Louvain-la-Neuve, Belgium

Photon interactions at the LHC result in striking final states with much lower hadronic activity in the central detectors than for *pp* interactions. In addition, the elastic exchange of a photon leads to a proton scattered at almost zero-degree angle. Tagging photon interactions relies on either the use of large rapidity gaps or on the detection of the scattered proton using very forward detectors. The studies related to such detectors are presented, including their characterization, their acceptance and reconstruction performance. Limitations due to the LHC beamline misalignment and possible solutions are also given.

1. Introduction

A significant fraction of *pp* collisions at the LHC will involve quasi-real photon interactions occurring at energies well beyond the electroweak energy scale [1]. The LHC can therefore be considered to some extend as a high-energy photon-proton or photon-photon collider. The initial comprehensive studies of high energy photon interactions at the LHC were recently reported [2, 3,4,5,6,7,8]. Clear identification of the remarkable photon-photon and photon-proton collisions out of the large sample of *pp* events requires good experimental *tagging* techniques. Two signatures characterizes the photon interactions: the presence of a very forward scattered proton and of a large pseudorapidity region of the detector, devoid of any hadronic activity, usually called *large rapidity gap* (LRG), in the forward directions.

During the phase of low luminosity (i.e. significantly lower than 10^{33} cm^{-2}s^{-1}), the *event pile-up* is negligible. Thanks to the colour flow in *pp* interactions between the proton remnant and the hard hadronic final states, a simple way to suppress generic *pp* interactions is to require LRGs. The LRG condition can be applied using a cut based on the energy measured in the forward detector containing the minimum forward activity ($3 < |\eta| < 5$). More details are given in [3]. Tagging photon interactions with LRG could rely only the central detector. But as the forward proton is not measured, the event final state is less constrained. At higher luminosity, the LRG technique cannot be used because of large event pile-up. Therefore the use of dedicated *very forward detectors* (VFDs) is mandatory in order to retain *pp* backgrounds low.

Both CMS and ATLAS experiments have extended their coverage in pseudorapidities to the forward regions [9]. This includes near-beam calorimeters and tracking detectors. The transport of particles through the LHC beamlines from the interaction point (IP) to the forward detectors is simulated with HECTOR [10]. The simulator is based on a linear approach of the beamline optics, implementing transport matrices from the optical element magnetic effective length, and with correction factors on magnetic strength for particles with non nominal energy. HECTOR deals with the computation of the position and angle of beam particles, and the limiting aperture of the optical elements. The measurement of the position and the angle of particles in dedicated near-beam very forward detectors, hundreds of meters away from the IP, helps in reconstructing the kinematics of the event at the related central detector. HECTOR links the information from very forward detectors (VFDs) to the one from the central detector, by precise calculation of the particle trajectory. The measurement in the central detector of exclusive dimuon final states, from $\gamma\gamma$ collisions or diffrac-

*E-mail: xavier.rouby@uclouvain.be.

tive photoproduction of Υ mesons, can be used for a very precise calibration of the VFDs [8].

2. Simulation techniques

2.1. Physical description

The simulator relies on a linear approach to single particle propagation. A beamline consists of a set of optical elements, amongst dipoles, quadrupoles, drifts, collimators, kickers and VFDs. The optical elements are described by their magnetic field, their length and their aperture. In turn, a set of particles, with all possible smearings of initial positions, angles or energies, is propagated by HECTOR through the beamline, particle by particle. The first terms of the Taylor expansion of the magnetic field can be interpreted as dipolar ($\frac{1}{R} = \frac{e}{p}B_y$), quadrupolar ($k = \frac{e}{p}\frac{\partial B_y}{\partial x}$) and sextupolar fields.

In the co-moving coordinate system, neglecting small deviations ($x \ll R$, $y \ll R$) and small momentum loss ($\Delta p \ll p$), this leads to the following equation of motions for a particle traveling along path length s through a magnetic element [**?**]:

$$\begin{cases} x''(s) + \left(\frac{1}{R^2(s)} - k(s)\right) x(s) = \frac{1}{R(s)}\frac{\Delta p}{p} \\ y''(s) + k(s)y(s) = 0. \end{cases} \quad (1)$$

The solution $(x(s), x'(s), y(s), y'(s))$ to these equations can be expressed as a linear combination of the initial values (x_0, x'_0, y_0, y'_0), where the rotation matrices are defined by the properties of the optical element (length and magnetic field). Each beam particle is represented by a phase space vector and each optical element by a transfer matrix by which the vector is multiplied. The propagation of a single particle is thus the *rotation* of the phase space vector by the n optical element matrices.

$$X(s) = X(0)\underbrace{M_1 M_2 ... M_n}_{M_{\text{beamline}}}$$

The whole beamline is modeled as a single transport matrix acting on each particle phase space vector (no intrabeam interactions). The optical element description also refers to its physical aperture. When a particle is propagated through an optical element, the compatibility between its trajectory and the optical element aperture is checked.

2.2. Implementation

Beam particles are described by a 6-components phase space vector $X = (x, x', y, y', E, 1)$, where (x, x') and (y, y') are the horizontal and vertical coordinates and angles; E is the particle energy. The sixth component is just a factor used to add an angular kick on the particle momentum direction. The optical elements (dipoles, quadrupoles, drifts, ...) are modelled by 6×6 transport matrices:

$$\mathbf{M_{units}} = \begin{pmatrix} \text{A} & \text{A} & 0 & 0 & 0 & 0 \\ \text{A} & \text{A} & 0 & 0 & 0 & 0 \\ 0 & 0 & \text{B} & \text{B} & 0 & 0 \\ 0 & 0 & \text{B} & \text{B} & 0 & 0 \\ \text{D} & \text{D} & 0 & 0 & 1 & 0 \\ K & K & K & K & 0 & 1 \end{pmatrix}$$

where

- A (and B) blocks refer to the action (focusing, defocusing, drift) on horizontal (and vertical, resp.) coordinate and angle.
- D terms reflect the dispersion effects of the horizontal dipoles on off-momentum particles.
- K factors are the angular action of kickers.

The *chromaticity*, or the energy dependence of the transport matrix, is implemented by rescaling the magnetic field terms (R, k, K) with a factor $(\frac{p}{p-\Delta p})$. The propagation of particles different from protons is also possible by rescaling these magnetic field terms:

$$k_i(\Delta E, q_p) = k_i \frac{p_0}{p_0 - \Delta p}\frac{q_p}{q_{\text{proton}}},\ k_i = R, k, K; \quad (2)$$

where q_p is the particle charge. Forward particles from the final state can be then propagated through the beamline via HECTOR.

3. Beamline simulation

Knowing the optics tables for both LHC beams, their trajectories can be compared simultaneously, in both top and side views, for the two

LHC beams aside (incoming beam 2 and outgoing beam 1, at the IP5 and IP1: Fig. 1). The top view shows the beams on the horizontal plane, clearly depicting the crossing angle at the IP5, and the beam separation after 70 m away from the interaction point. The bending of the sector dipoles has been switched off in order to makes graphics more clear – this is why both beams are straight and parallel after 250 m. However, the optical elements have been shifted (without tilt) in the horizontal plane by the half of the beam separation distance, from 180 m away from the IP, in order to match the ideal beam path: a proton with nominal energy and on the ideal orbit should travel through optical elements in their geometrical center. The side view in turn shows the beams in the vertical plane. In addition, the major optical elements have been drawn: rectangular dipoles in red, sector dipoles in light green, and quadrupoles in yellow and blue.

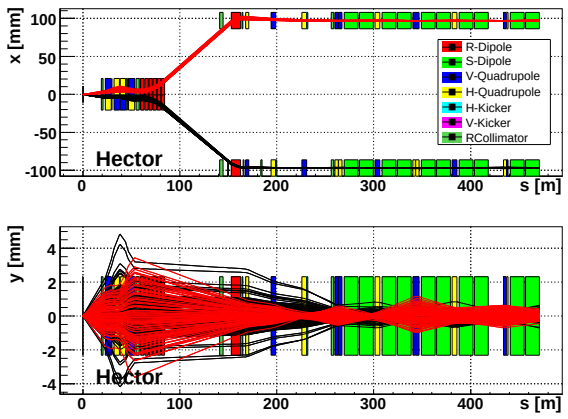

Figure 1. Top and side views of both LHC beams around the IP5. The IP is located at $s = 0$ m. Beam 2 (red) flows from the right to the left and is seen before its passage at the IP. Beam 1 (black) is seen downstream, passing from the left to the right after the crossing. In this graph, the bending effect of the sector magnets (S-Dipoles) has been switched off, thus rectifying the beam path to a straight line after 250 m [10].

The simulation of proton beams is needed for the validation of the simulator results, by a direct comparison to the results of other simulators.

3.1. Calibration

The calibration of the reconstructed variables at forward detectors can be well maintained using the physics processes and the central detectors. At HERA, for example, the elastic ρ meson photoproduction was used where the momentum of the scattered proton could be deduced from two decay charged pions using the central tracking. At the LHC, the two-photon exclusive production of dimuon pairs and the diffractive Υ photoproduction seems good calibration processes [7,8], with large statistics for the detectors at 420 m. The visible cross section of exclusive dimuons is large ($\sigma \leq 7$ pb), including the acceptance of central detectors. The measurement of the final state muon pair provides an estimate of the proton energy loss $x = E_\gamma / E_{\rm beam}$, which can be matched with the proton position in the VFDs. From the dimuon longitudinal momentum P_z and invariant mass $M_{\mu\mu}$, one gets

$$E_\gamma = \pm\frac{P_z}{2} + \frac{\sqrt{(M_{\mu\mu})^2 + (P_z)^2}}{2}.$$

This should allow for a run-by-run calibration of the scattered proton energy scale within a full acceptance range. Finally, the expected reconstruction power of central detectors is excellent for such dimuon events, giving the proton energy uncertainty about 10^{-4} per event [11]. Recent results with the full similation of the detector show even better resolutions, at the order 5×10^{-6} (depending on x) [8]. One should note, however, that using this process it is not possible to check the angular reconstruction, and that it has much more limited statistics within acceptance of the detectors at 220 m.

4. Very Forward Detectors

In the following, the use of very forward detectors (VFDs) located at 220 m and 420 m from IP5 are discussed, as taggers for photon interactions. The assumed location of the first detector is ($s = 220-224$ m, $x = 2000\ \mu$m), and of the second one at ($s = 420 - 428$ m, $x = 4000\ \mu$m). No

hypothesis is made on their detection efficiency or their resolution, unless quoted. We consider here VFDs providing 2D-measurement (x and y coordinates), each consisting in fact of two stations separated by 4 and 8 m as a lever arm for the angle measurement, with no magnetic element in between.

4.1. Acceptance

Using HECTOR's aperture description, it is possible to identify the characteristics of the protons that will hit the VFD. The exchange of a photon, leaving the proton intact, results in a proton energy loss (E_{loss}) and a scattering angle, directly linked to the four-momentum transfer squared (t), or equivalently to the photon virtuality (Q^2). The acceptance windows of the VFDs can be computed by performing scans in (E_{loss}, t) and computing the probabilities of reaching the detectors. The figure 2 shows the contour plots of the detectors acceptance, in this (E_{loss}, t) plane. The VFD acceptances mostly depend on E_{loss}, and have a very small sensitivity in t, within a large t range. Corresponding profile at fixed virtuality is shown in figure 3.

The total diffractive cross-section at the LHC is very large, resulting in a high rate of diffractive protons hitting the VFDs. As a result, it causes extremely high irradiation levels. About 10^{14} hits/cm^2 are expected per year at low luminosity. This illustrates the need for very radiation hard detectors.

4.2. Chromaticity grids

Once the acceptance windows of very forward tracking detectors are defined, it is interesting to see matching between the proton variables at the IP and those measured by VFDs. Depending on their energy and angle at the IP, forward protons will hit the VFDs at various positions. Drawing iso-energy and iso-angle curves for a set of sample protons produces a grid in the measurement related variables, (x_1, x_2) or (x_1, θ). Due to optics of the LHC beamlines, the grid unfolds itself in a much clearer way in the latter plane, and is almost invisible in the former one. The energy dependence of the transfer matrices implies a deformation of the grid – without such a dependence, the grid would be a parallelogram. One should note, that uncertainty of the transverse position

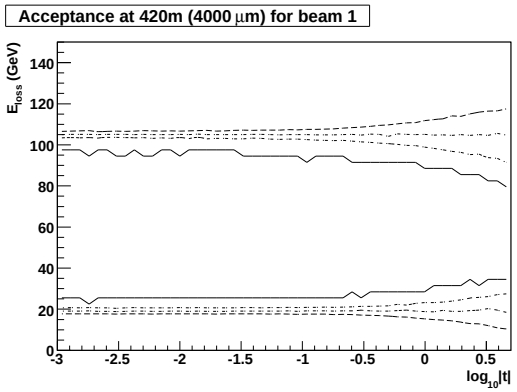

Figure 2. VFD proton acceptance for the LHC beam 1 around the IP5. The VFD is located at (s = 420 m, x = 4000 μm). This map shows contours of 25%, 50%, 75% and (plain curve) 100% acceptance. The acceptance is roughly rectangular, i.e. independent of t. The angular kick coming from the large momentum transfers leads to an increasing smearing of the graph lower edge [10].

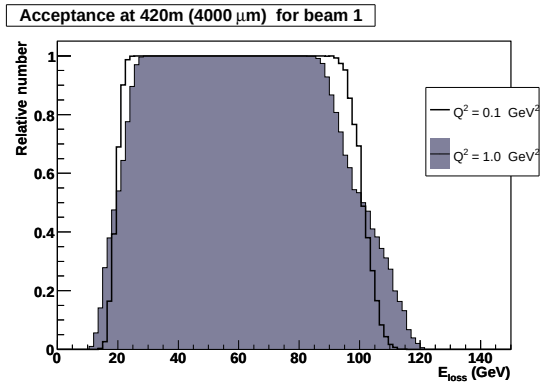

Figure 3. VFD acceptance as a function of energy loss, for two fixed virtualities (Reminder: $Q^2 = -t$). See previous figure for more details [10].

of the proton vertex at the IP results effectively in smearing the chromaticity grids. Anyway, these chromaticity grids provide a straightforward tool for unfolding the energy and angle at the IP of the measured particle. The grid in figure 4 is calculated in the energy range accessible to the VFDs.

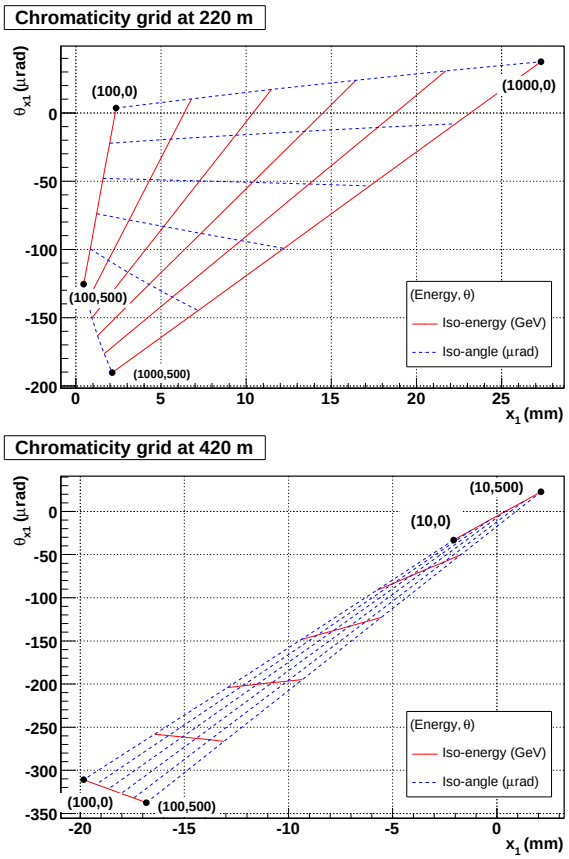

Figure 4. Chromaticity grids: iso-energy and iso-angle lines for the VFDs at 220 m (*above*) and 420 m (*below*) away from the IP5, for the LHC beam 1. The graphs show the positions x_1 and angle θ_{x1} of protons, given the energy loss $[0; 1000]$ GeV and the angular kick of $[0; 500]$ μrad. The energy dependence of the transfer matrices induces a deformation of the grid, worsening the reconstruction power at higher angles [10].

4.3. Reconstruction

The reconstruction of the event kinematics is possible with HECTOR, from the VFD measurements. If a beam particle has exchanged a photon at the IP, one could reconstruct photon's energy (E) and virtuality (Q^2). The particle energy at a given position in the beamline is obtained from the measured particle position and angle within the matrix formalism by solving these equations:

$$\begin{cases} x_s = a_s x_0 + b_s x'_0 + d_s E \\ x'_s = \alpha_s x_0 + \beta_s x'_0 + \gamma_s E \end{cases}$$

The transfer matrix of the beamline yields the coefficients a, b, etc. The introduction of an energy dependence on the strength of optical elements refines the transfer matrix, becoming a function of E: $a_s(E)$, $b_s(E)$,... This dependence will introduce *non linearities*.

Neglecting the terms $a_s x_0$ and $b_s x'_0$ leads to significant sensitivity to the non-nominal values of the average vertex position and beam direction (*tilt*) at the IP. While the average vertex position can be very well measured using the central detectors, the beam tilt is more difficult to control – it should be known to better than $10 - 20$ μrad to avoid causing a significant bias. One can reconstruct the energy and scattering angles using position measurements at two detector stations at the same time. This requires to solve the equations for x_s at both detectors for E. The a_s, b_s and d_s coefficients of the transfer matrix depend on energy with rather complicated shapes, as they are products of many magnets matrices. One efficient way to get those is then simply to fit each coefficient as a function of energy. Various fitting functions were tried, but a quadratic fit proved to be sufficient to avoid any visible bias or resolution degradation.

Using these fitted coefficients, one can easily get a formula for x_0 as a function of x at both detectors and of the energy. For each pair of detector x coordinates, the used method is to numerically find the root ($x_0 = 0$) of the formula to get the energy corresponding to a $x_0 = 0$, and thus neglect the interaction point transverse extension.

This method allows to get reconstructed energy independently of the angle of the particle at the

IP. Energy reconstruction resolutions does not degrade anymore if the particle transverse momentum p_T rises, but the price to pay is that the detectors resolutions become critical. In particular, it means that the uncertainty of the reconstructed angle at a given detector location should be better than the beam angular divergences there (6 and 1.5 μrad, respectively). The transverse momentum can thus also be computed from the matrix coefficients once the energy has been reconstructed.

The reconstructed energy resolution stays very good even with non-negligible initial particle p_T. Figures 5 and 6 show the p_T and energy dependence of resolutions on the transverse momentum and energy, for various detectors resolutions. As expected, the energy resolution is independent of p_T but is sometimes sensitive to the energy as expected from the chromaticity grids of Fig. 4. The effect of the detector resolution, which was absent for the simple reconstruction method described previously, is now clearly visible even for an excellent resolution of 5 μm, especially for detectors at 220 m from IP.

In summary, the proton angular distribution at the IP affects the most the energy reconstruction. In contrast, the vertex lateral distribution has negligible impact. As a result, the most important beam parameter, which can change run-to-run, is the beam tilt at the IP. In principle, it can be indirectly controlled by the beam position monitors (BPMs) at 220 and 420 m, but more direct tilt measurements are favored, as by using BPMs next to the IP, or by monitoring the direction of neutral particle (photons, neutrons, or neutral pions) production in the zero-degree calorimeters (ZDCs).

The energy resolution squared of the scattered proton σ_E can be then approximately decomposed into four terms:

$$\sigma_E^2 = \sigma_0^2 + \sigma_{vtx}^2 + \sigma_{ang}^2 + \sigma_{det}^2,$$

where the nominal beam energy dispersion $\sigma_0 \approx 0.8$ GeV, the contribution due to the vertex spread $\sigma_{vtx} \approx 0.7$ GeV at 420 m and $1-2$ GeV at 220 m, the contribution due to the detector resolution, neglecting the angular effects, σ_{det}^2 is small for resolutions better than 50 μm, and the contribution due to the proton non-zero angle at the IP, σ_{ang}, which is very sensitive the angular reconstruction at the VFDs; even for a zero-degree scattering if one neglects effects due to the beam angular divergence at the IP, $\sigma_{ang} \approx 1$ GeV at 420 m and ≈ 3 GeV at 220 m.

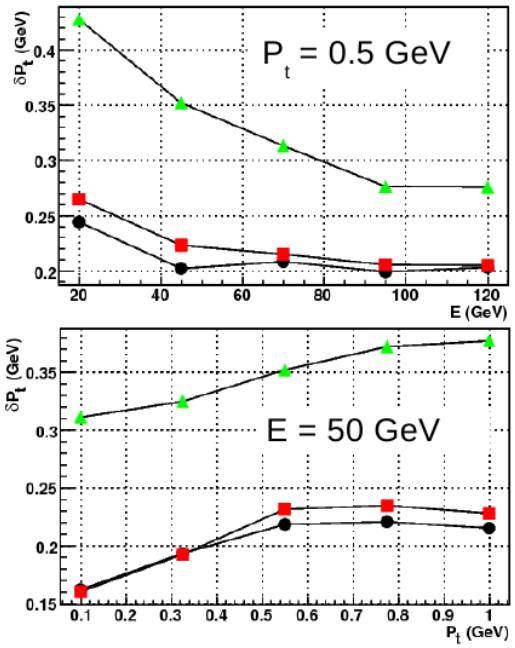

Figure 5. Resolution of the reconstruction of the particle transverse momentum p_T, as a function of the energy loss (*above*) and of the transverse momentum (*below*), for VFDs at 420 m from the IP5. Dots correspond to different scenarios of detectors resolutions, namely perfect detectors (*circles*), 5 μm (*squares*) and 30 μm (*triangles*) spatial resolution [10].

5. Misalignments

The misalignment of LHC optical elements could have a significant impact on the measurements with very forward detectors. As the deflection of the particle paths depends on their po-

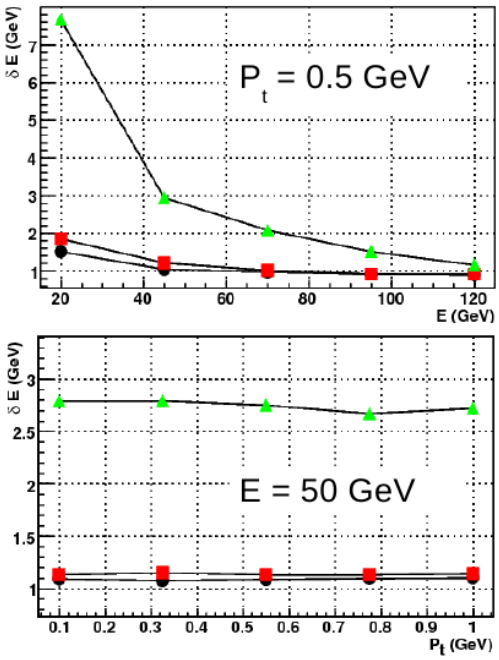

Figure 6. Resolution of the reconstruction of the particle energy loss E, as a function of the energy loss (*above*) and of the transverse momentum (*below*), for VFDs at 420 m from the IP5. Dots correspond to different scenarios of detector resolutions, namely perfect detectors (*circles*), 5 μm (*squares*) and 30 μm (*triangles*) spatial resolution [10].

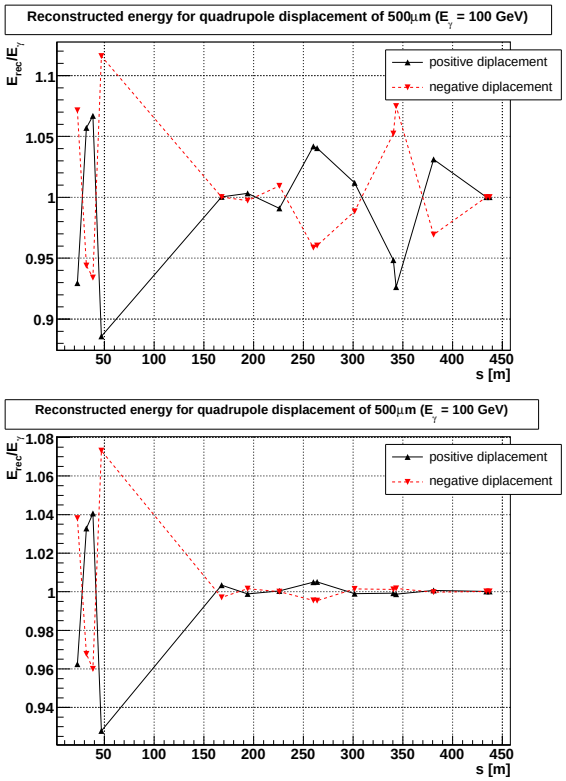

Figure 7. The misalignment of the LHC quadrupoles bias the energy reconstruction. The graphs show the bias for the reconstruction (with the trivial method) of a 100 GeV energy loss assuming the misaligned quadrupoles at various positions. Each element is separately shifted (500 μm) , assuming a perfect alignment for the rest of the beamline. The impact of the misalignment can be important. Even a perfect knowledge of the actual beam position at the VFD (*below*) does not compensate for this bias, depending on the position of the misplaced quadrupole [10].

sitions in quadrupoles, a misplacement of these optical elements implies a change in the nominal beam position. In turn, as the accurate position measurement with the forward tracking detectors (as well as the information inferred from the segmentation of forward calorimeters) is referred to the ideal beam location, changing this reference results in a biased reconstruction of the measured particles.

Figure 7 shows the impact of possible shifts (0.5 mm) of the beamline quadrupoles on the energy reconstruction with VFDs at 420 m. The reconstruction assumes ideal beamline in which only one quadrupole at a time is separately moved. Effects even higher than 10 % could be expected. Similar results are observed due to the beam tilts at the IP [10]. One can partially correct for these effects using information from the beam position monitors, but better results are obtained using a physics calibration process like the

two-photon muon pair exclusive production or the diffractive photoproduction of Υ, at least in case of the VFDs at 420 m [8].

These misalignment effects and the corrections are illustrated (Fig. 8) by the study of two-photon exclusive production of the SM Higgs boson ($pp \to pp(\gamma\gamma)H$) with $M_H = 115$ GeV. The measurement of the energy of two scattered protons straightforwardly yields the boson mass, by means of the so-called *missing mass method*. As a consequence, an uncorrected measurement with misalignment leads to a bad mass calculation. A quadrupole (MQXA1R5, $s = 29$ m) close to the IP is shifted by 500 μm. The misalignment-induced change in the VFD acceptance is visible. The limitations of the beam-position-based corrections are clearly visible, even assuming no systematic errors, while the muon-calibration stays unbiased (though only a relatively small sample of 700 dimuon events was used to get the correction factors).

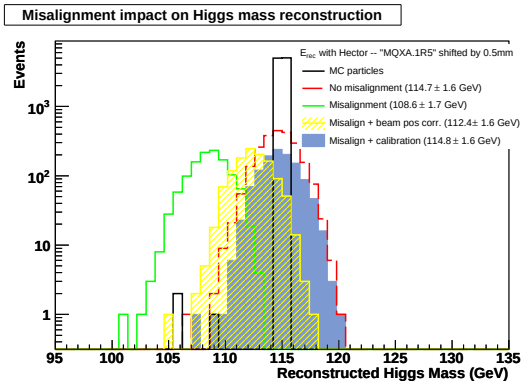

Figure 8. Illustration of the effects in the energy reconstruction due to the misalignment of LHC quadrupoles. The graphs show the reconstructed Higgs boson mass in the two-photon exclusive production, using energy of two forward scattered protons. Misaligning a quadrupole (MQXA1R5, $s = 29$ m) close to the IP leads to a loss of acceptance. The reconstructed values including the correction due to the dimuon calibration are also plotted. In brackets, the average reconstructed mass and its resolution are given, without including the beam energy dispersion [10].

6. Summary and outlook

Photon interactions at the LHC result in striking final states with much lower hadronic activity in the central detectors than for pp interactions. While forward rapidity gaps can be used for their tagging in a low pile-up environment, the use of very forward detectors is mandatory for luminosity starting at $\mathcal{L} = 2 \times 10^{33}$ cm^{-2}s^{-1}. The good simulation of particle transport in the LHC beamline is very important. It allows to characterize the detectors and to reconstruct the event from the scattered proton measurement. Impact of beamline misalignement has been studied as well as the calibration possibilities from the observation of exclusive dimuon final states.

REFERENCES

1. K. Piotrzkowski, "Tagging two-photon production at the CERN Large Hadron Collider", *Phys. Rev. D*, **63**, 071502 (2001).
2. J. de Favereau et al., "High energy photon interactions at the LHC ", CP3-08-04, hep-ph/xxxxxxxx, June 2008.
3. S. Ovyn, "Associated W and Higgs boson photoproduction and other electroweak photon induced processes at the LHC", these proceedings, arXiv:0806.1157 [hep-ph].
4. N. Schul, K. Piotrzkowski "Detection of two-photon exclusive production of supersymmetric pairs at the LHC", these proceedings, arXiv:0806.1097 [hep-ph].
5. T. Pierzchala, "Sensitivity to anomalous quartic gauge couplings in photon-photon interactions at the LHC", these proceedings.
6. J. de Favereau, "Single top quark photoproduction at the LHC ", these proceedings.
7. J.J. Hollar, "$\gamma\gamma \to \ell^+\ell^-$ and $\gamma p \to \Upsilon p \to \ell^+\ell^- p$ at CMS", these proceedings, CMS CR-2008/026.
8. X. Rouby, "Measurements of photon induced processes in CMS and forward proton detection at the LHC", PhD dissertation, UCL, July 2008.

9. M. Grothe, "Forward detectors around the CMS interaction point at LHC and their physics potential", these proceedings, CMS CR-2008/033.
10. X. Rouby, J. de Favereau, K. Piotrzkowski, "HECTOR, a fast simulator for the transport of particles in beamlines", *JINST*, **2**, P09005 (2007).
11. M.G. Albrow *et al.*, "Prospects for Diffractive and Forward Physics at the LHC", CERN/LHCC 2006-039/G-124.

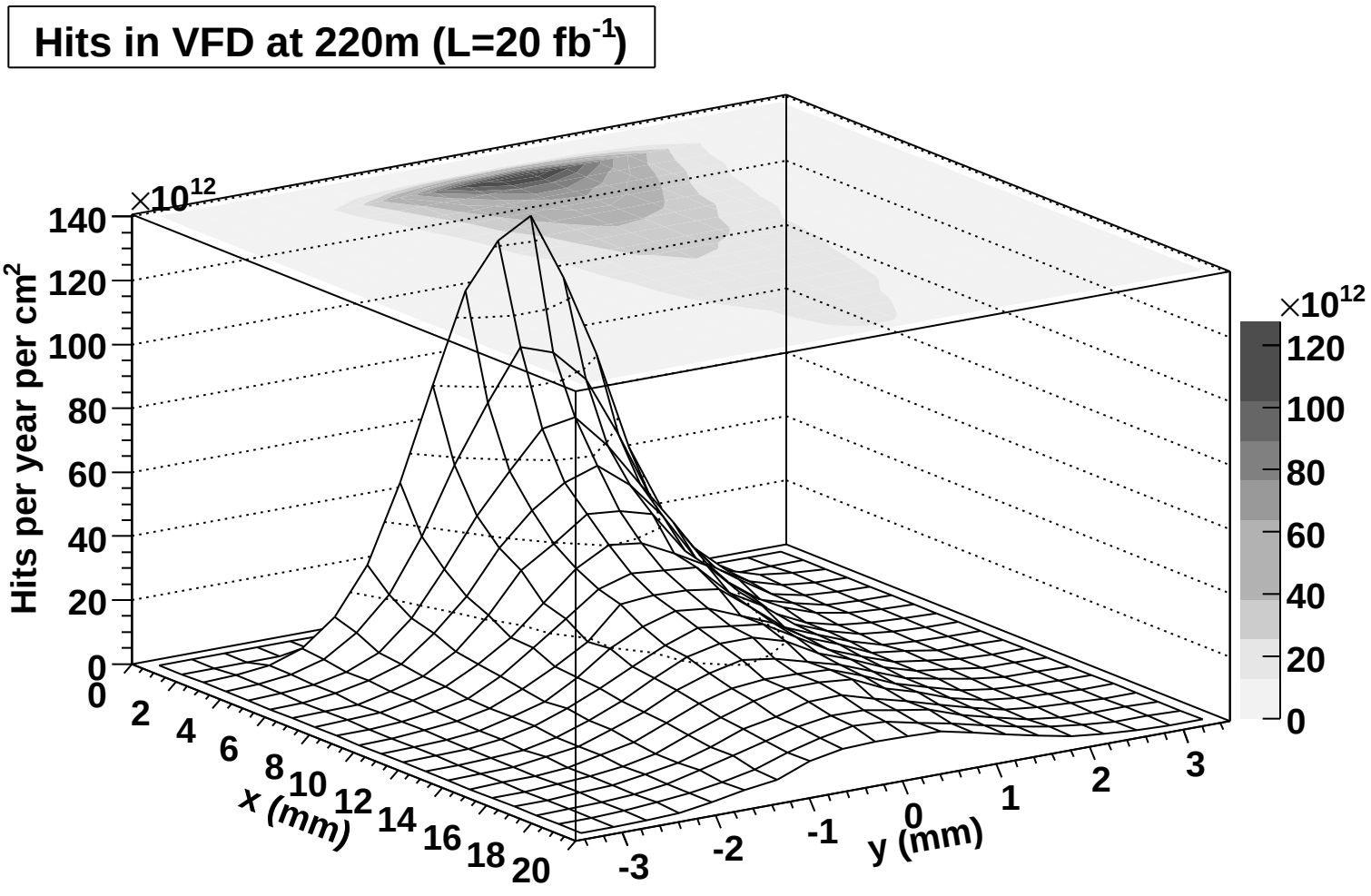
Hits in VFD at 220m (L=20 fb-1)
×10^12
Hits per year per cm2
140
120
100
80
60
40
20
0
0
2
4
6
8
10
12
14
16
18
20
x (mm)
-3
-2
-1
0
1
2
3
y (mm)
×10^12
120
100
80
60
40
20
0

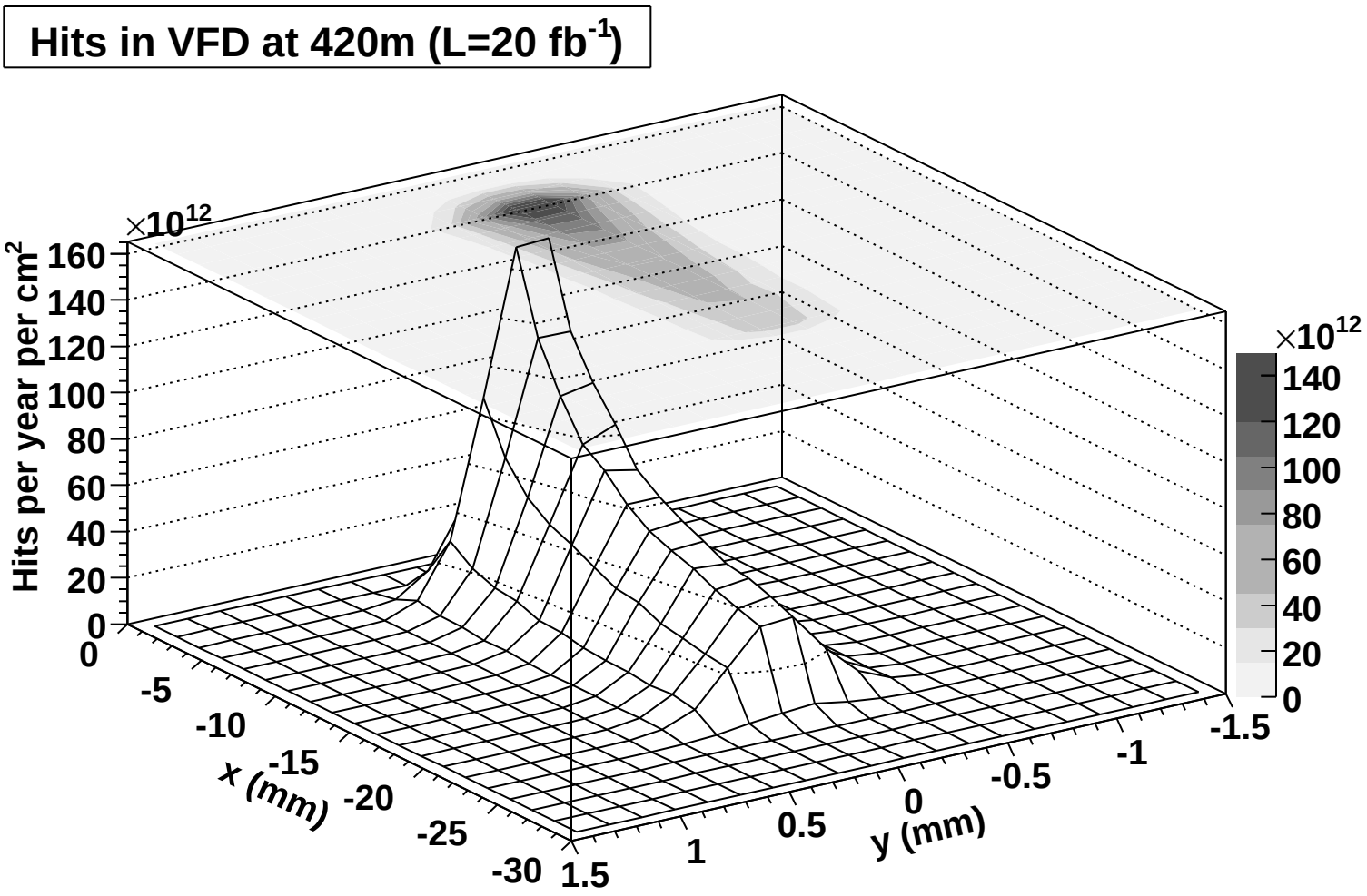
Hits in VFD at 420m (L=20 fb-1)
×10^12
Hits per year per cm2
160
140
120
100
80
60
40
20
0
0
-5
-10
-15
-20
-25
-30
x (mm)
1.5
1
0.5
0
-0.5
-1
-1.5
y (mm)
×10^12
140
120
100
80
60
40
20
0

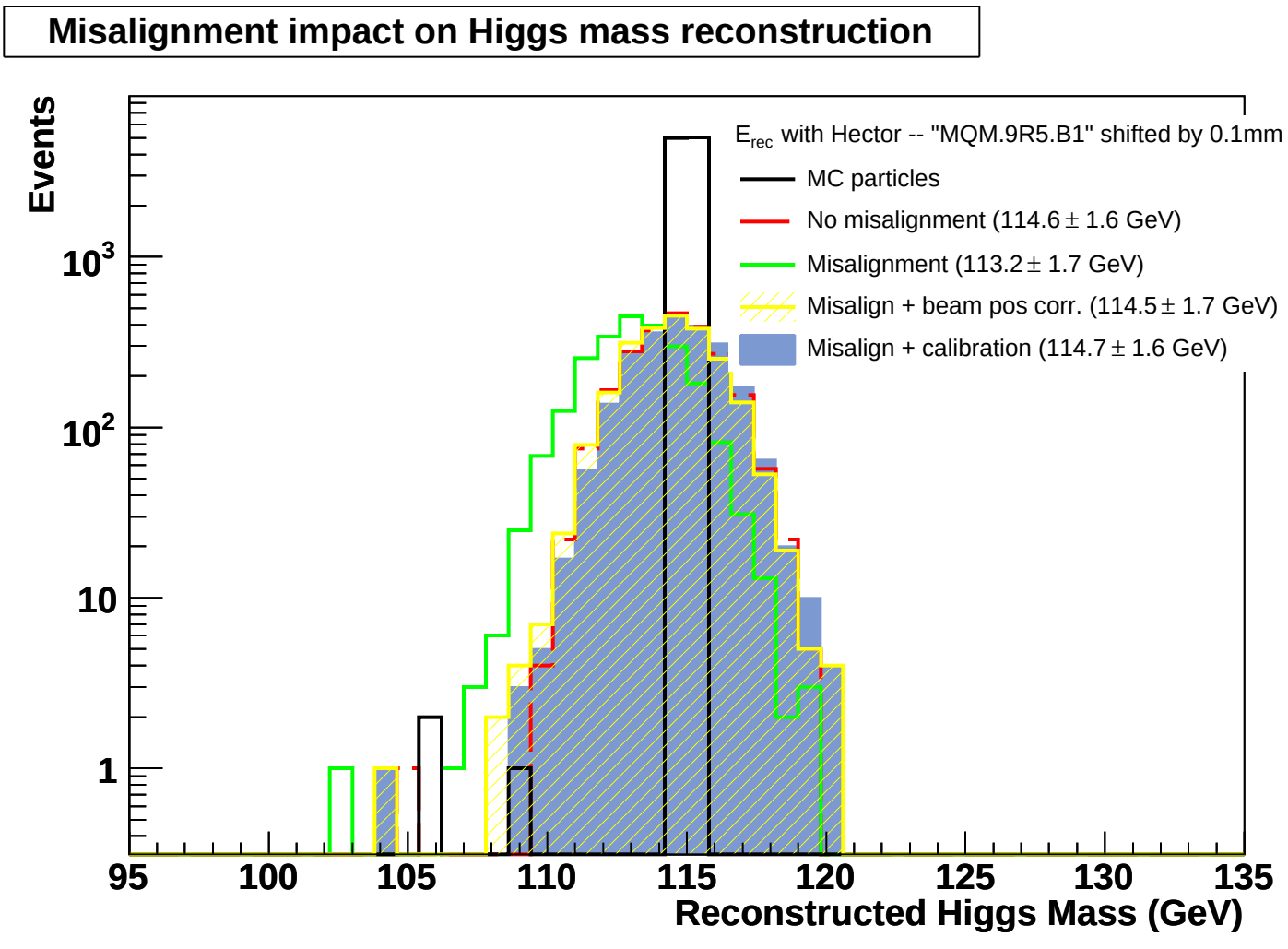
Misalignment impact on Higgs mass reconstruction
Events
10^3
10^2
10
1
95
100
105
110
115
120
125
130
135
Reconstructed Higgs Mass (GeV)
E_{rec} with Hector -- "MQM.9R5.B1" shifted by 0.1mm
MC particles
No misalignment (114.6 ± 1.6 GeV)
Misalignment (113.2 ± 1.7 GeV)
Misalign + beam pos corr. (114.5 ± 1.7 GeV)
Misalign + calibration (114.7 ± 1.6 GeV)